Supporting information

Regulation of closed pores in hard carbon for enhanced electrochemical sodium storage

Ziying Zhang[a], Yingxinjie Wang[b], Kejian Tang[a], Zerui Chen[b], Xiaohui Li[b], Nan Zhang[b], Zhenjun Wu*[a], Xiuqiang Xie*[b]

[a] College of Chemistry and Chemical Engineering, Hunan University, Changsha 410082, P. R. China. E-mail: wooawt@hnu.edu.cn.

[b] College of Materials Science and Engineering, Hunan University, Changsha 410082, P. R. China. E-mail: xiuqiang_xie@hnu.edu.cn.

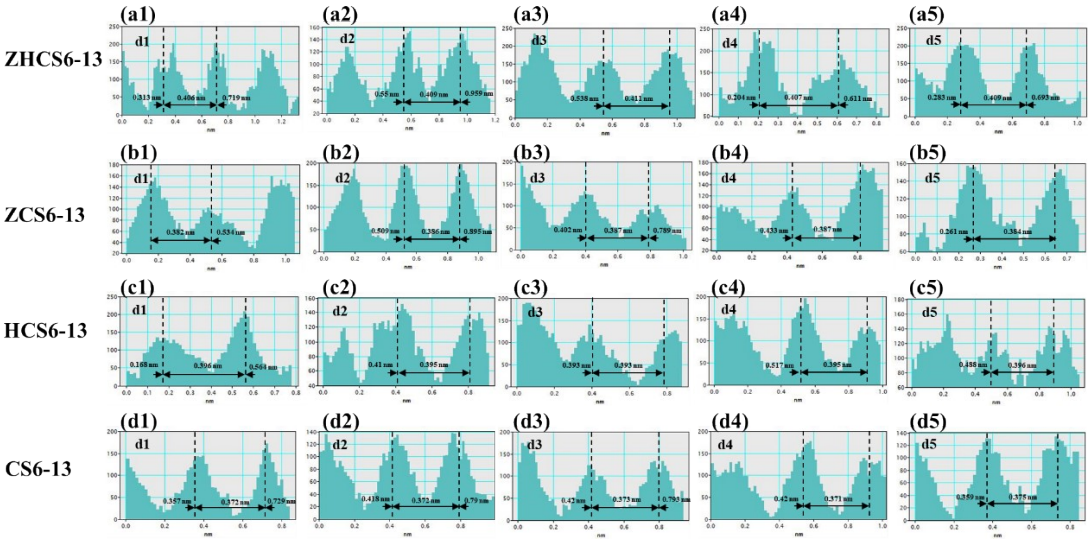

Fig. S1. The measured interlayer distance from TEM of (a1-a5) ZHCS6-13, (b1-b5) ZCS6-13, (c1-c5) HCS6-13, and (d1-d5) CS6-13.

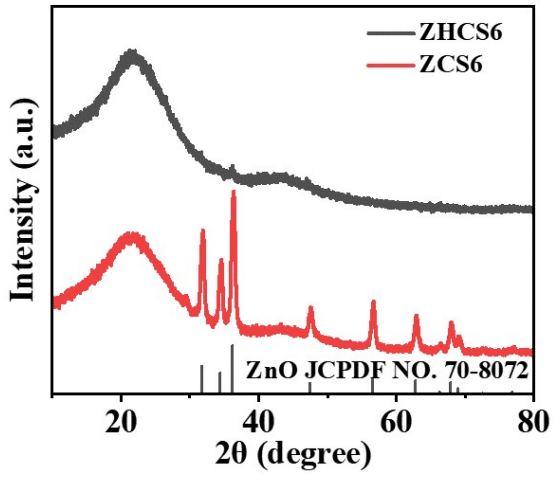

Fig. S2. XRD patterns of ZHCS6 and ZCS6.

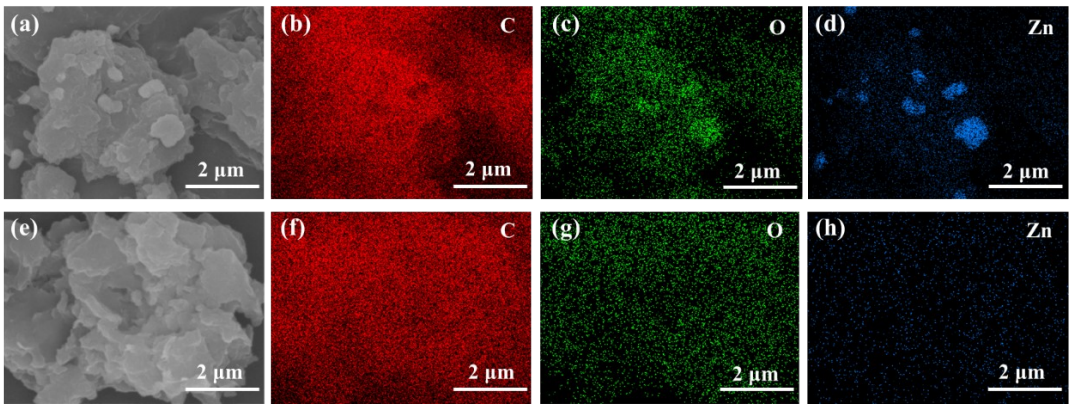

Fig. S3. SEM image and the corresponding EDS mappings of (a-d) ZCS6, (e-h) ZHCS6.

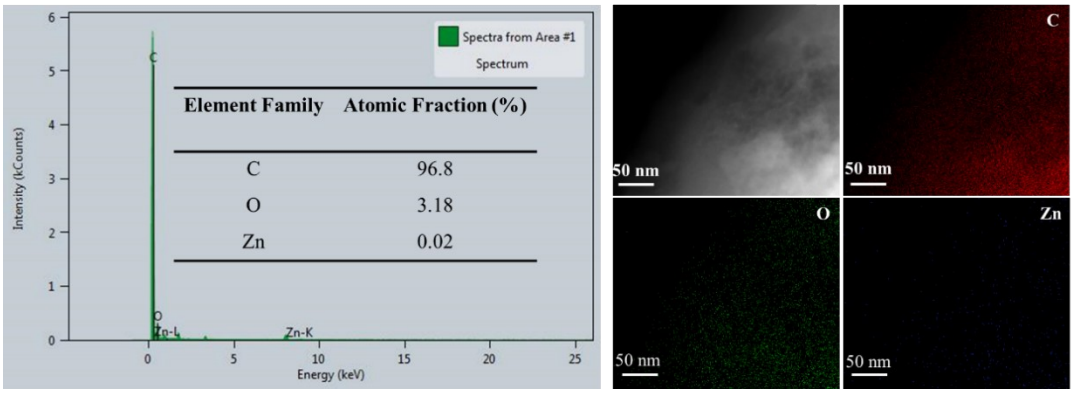

Fig. S4. TEM-EDS spectra and EDS mapping of ZHCS6-13.

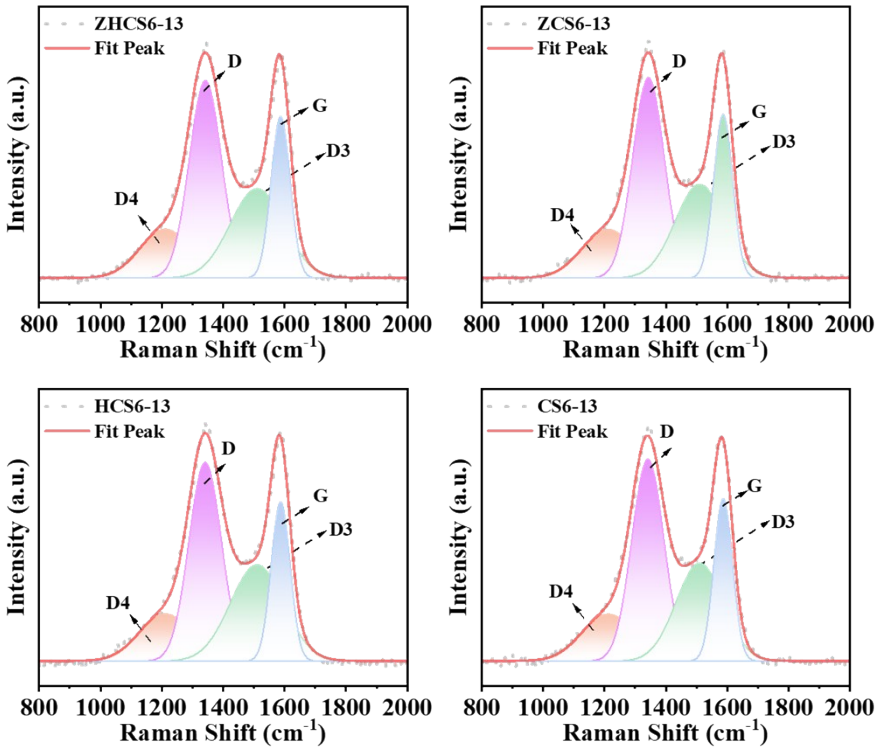

Fig. S5. Fitted Raman spectra of ZHCS6-13, ZCS6-13, HCS6-13, CS6-13.

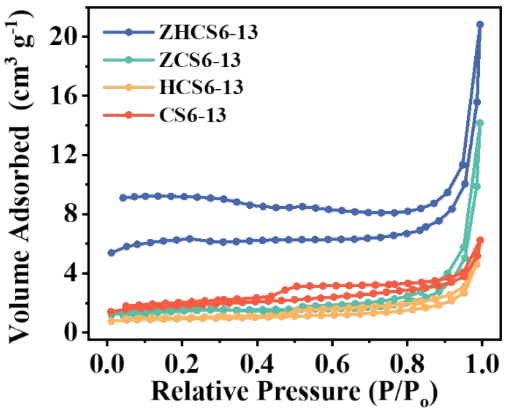

Fig. S6. N_2 adsorption-desorption isotherms.

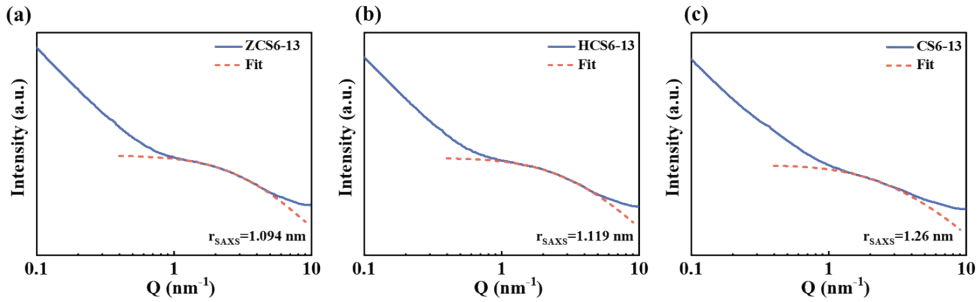

Fig. S7. (a-c) Fitted SAXS patterns of ZCS6-13, HCS6-13 and CS6-13.

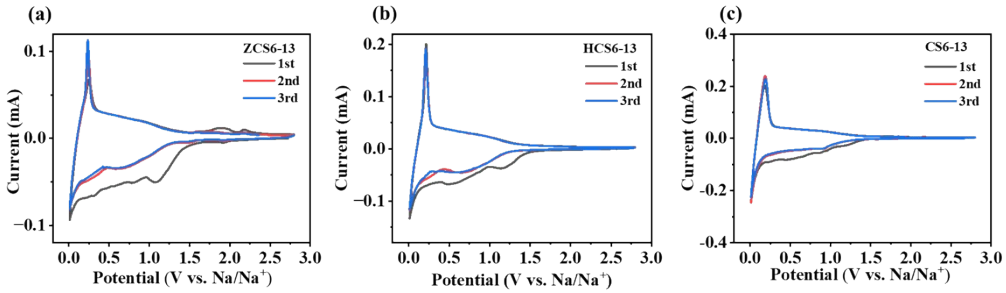

Fig. S8. (a-c) CV curves of ZCS6-13, HCS6-13 and CS6-13 at 0.1 mV s^{-1}.

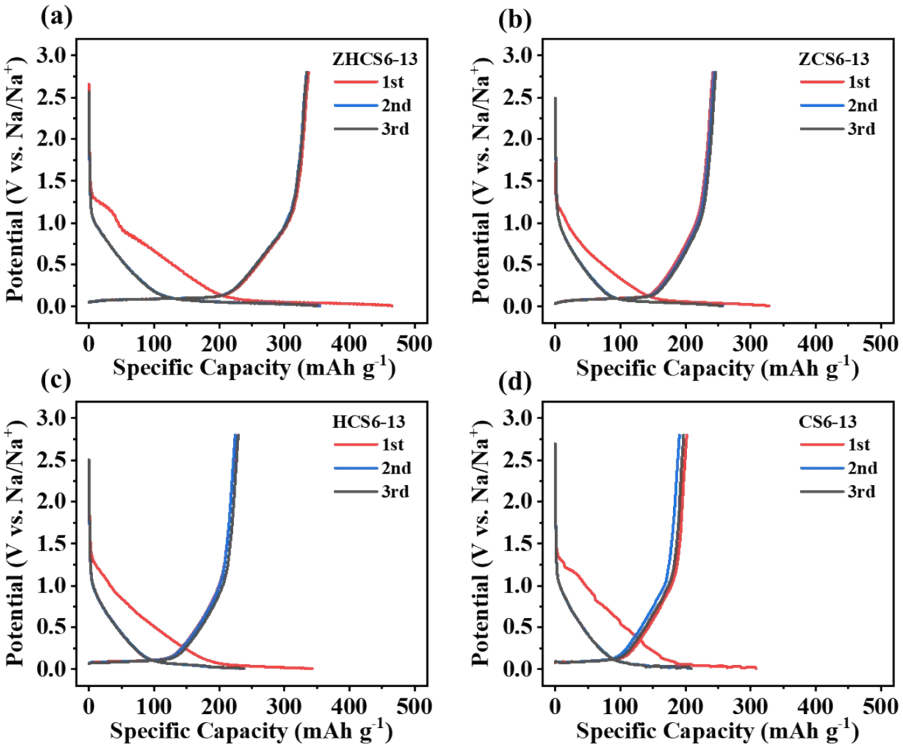

Fig. S9. Galvanostatic charge/discharge profiles of (a) ZHCS6-13, (b) ZCS6-13, (c) HCS6-13, and (d) CS6-13 at a current rate of 25 mA g^{-1}.

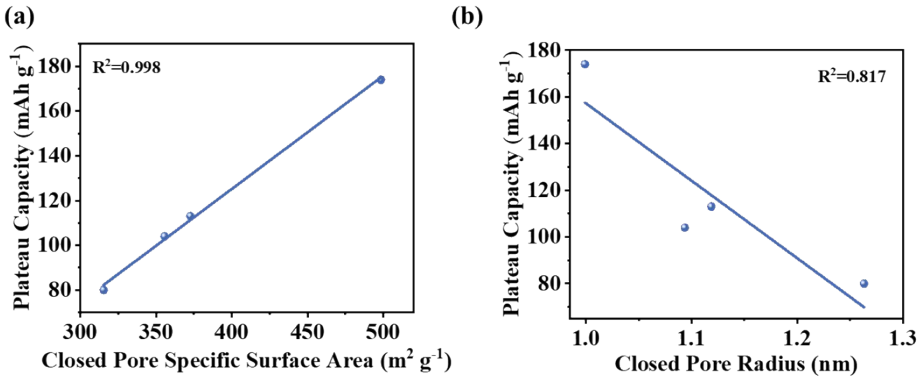

Fig. S10. The relationships between plateau capacities and closed pore specific surface area/r_{SAXS}.

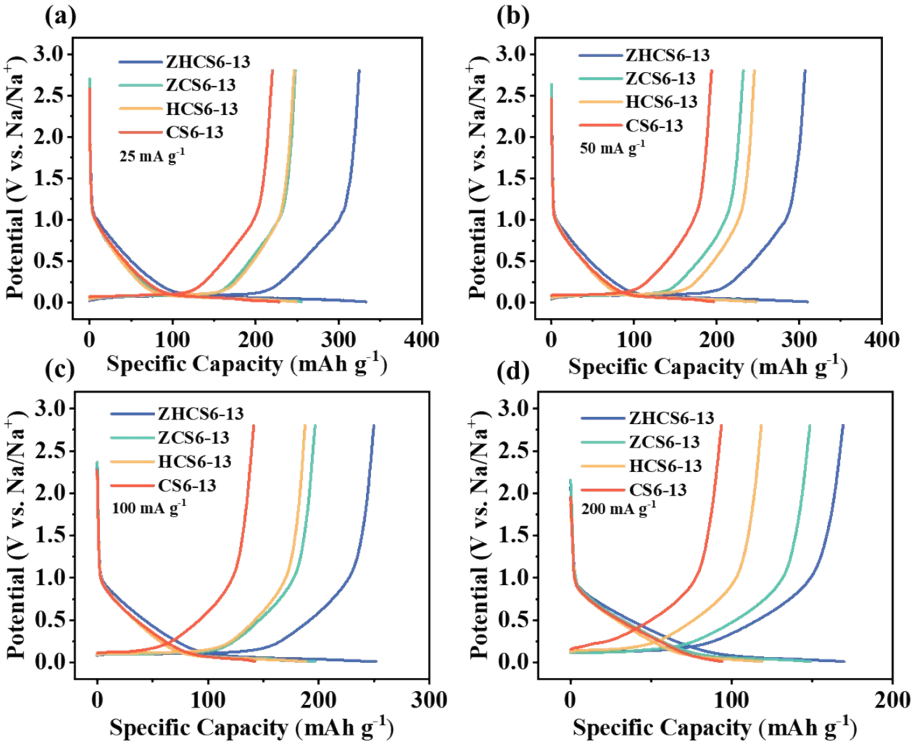

Fig. S11. GCD curves at (a) 25, (b) 50, (c) 100, and (d) 200 mA g^{-1}.

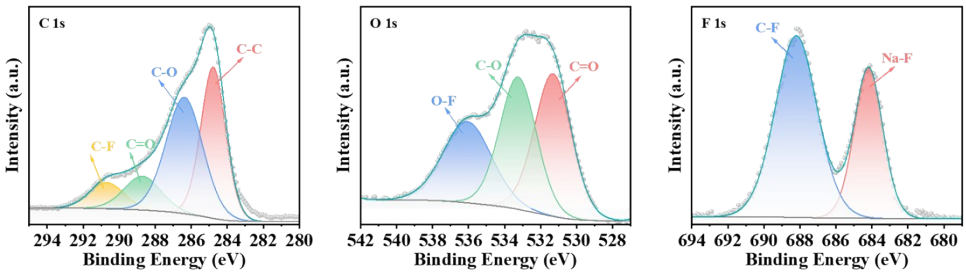

Fig. S12. Interfacial chemistry of ZHCS6-13. The high-resolution XPS spectra of (a) C 1s, (b) O 1s, and (c) F 1s collected at the ZHCS6-13 electrodes after 100 cycles at 50 mA g^{-1}.

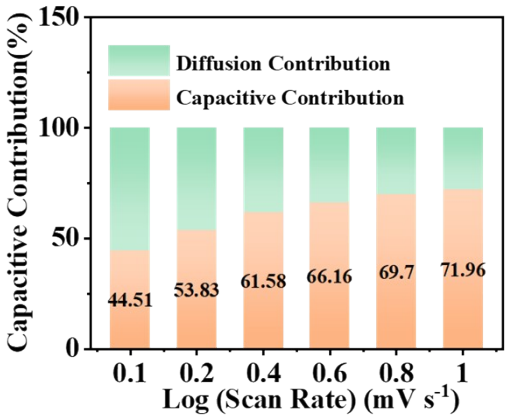

Fig. S13. Capacitive contribution percentage of ZHCS6-13 at various scan rates.

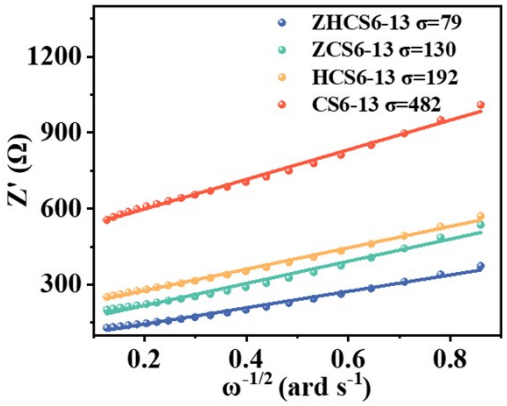

Fig. S14. The linear fits of Z' to $\omega^{-1/2}$ in the low-frequency region.

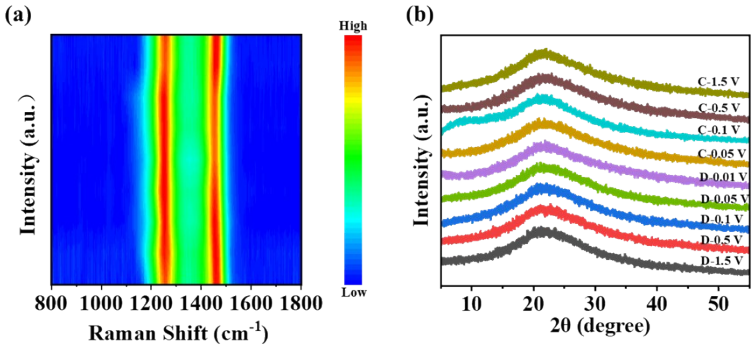

Fig. S15. (a) the ex-situ Raman contour plot and (b)the ex-situ XRD of the ZHCS6-13 electrode.

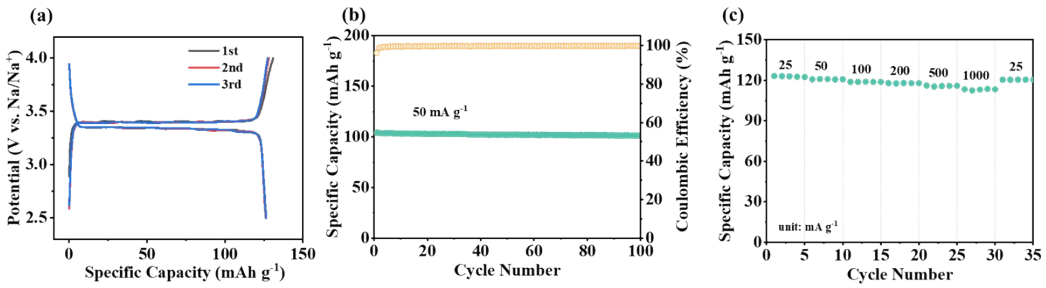

Fig. S16. (a) The GCD profiles of NVP half-cell at 25 mA g^{-1}. (b) Cycling performance and (c) rate of commercial NVP cathode in Na half-cells.

Table S1. Structure parameters of hard carbon materials.

Sample	D_{002}（nm）	La（nm）	Lc（nm）	A_D/A_G	S_{BET} ($m^2\ g^{-1}$)	r_{SAXS}（nm）	$S_{closed\ pore}$ ($m^2\ g^{-1}$)
ZHCS6-13	0.4	4.25	0.99	2.05	12.700	0.999	499
ZCS6-13	0.39	4.35	1.00	2.03	5.890	1.094	356
HCS6-13	0.39	3.95	0.96	2.14	3.467	1.119	373
CS6-13	0.37	4.20	0.98	2.13	6.626	1.260	315

(1) D_{002}: Interlayer distances calculated by XRD.

(2) The Scherrer equations were used to calculate the average graphite domain length (L_a) and the graphite crystallite thickness (L_c)[1]. The specific expressions are as follows:

$$L_a = \frac{1.84\lambda}{B_{100}COS\theta_{100}} \quad \text{(equation S1)}$$

$$L_c = \frac{0.89\lambda}{B_{002}COS\theta_{002}} \quad \text{(equation S2)}$$

Where λ is the wavelength of the X-rays (0.15418 nm), B_{100} and B_{002} are the full width at half maximum (FWHM) value of the (100) and (002) peaks, and $2\theta_{100}$ and $2\theta_{002}$ are the diffraction angle.

(3) The mid-angle region of the SAXS data (1 to 10 nm^{-1}) was fitted based on the semi-empirical Teubner-Strey model, to obtain more detailed structural information about the internal pores structure[2, 3]. The specific expressions are as follows:

$$I_{mp} = I_0 \frac{1}{1 + C_1Q^2 + C_2Q^4} \quad \text{(equation S3)}$$

Where I_0, C_1 and C_2 are tunable constants, the following structural parameters can be further calculated.

$$r_{saxs} = \sqrt{5C_1} \quad \text{(equation S4)}$$

$$S_{closed\ pore} = I_0 \frac{1}{C_2 2\pi(\Delta SLD)^2} \quad \text{(equation S5)}$$

$$\Delta SLD = \rho_{graphite} \frac{d_{002}}{d_{002}^{graphite}} \left(\frac{d_{100}}{d_{100}^{graphite}} \right) \quad \text{(equation S6)}$$

Where r_{saxs} is the average pore radius. $S_{closed\ pore}$ are the total specific surface areas（including open and closed pores）. ΔSLD is the structural density, where d_{002} is the interlayer distance and d_{100} is in-plane distance. The fitting results are shown in Table S1.

Table S2. Equivalent circuit fitting calculation results of EIS.

Sample	R_S (Ω)	R_{ct} (Ω)
ZHCS6-13	3.91	113
ZCS6-13	4.04	188
HCS6-13	2.29	245
CS6-13	4.00	590

Table S3. Electrochemical performance of hard carbon anodes prepared from different biomass precursors for SIBs.

Biomass precursor	ICE (%)	Reversible capacity (mA h g^{-1})	Plateau capacity (<0.1V vs. Na^+/Na) (mA h g^{-1})	Current density (mA g^{-1})	Reference
ZHCS6-13	73	340	174	50	This work
NDC-1000 (walnut shell)	-	257	157	50	4
HC-W (walnut shells)	66	315	175	50	5
P1000 (pistachio shell)	74.9	225	-	10	6
HC-1000 (Bagasse)	73.1	331.3	156.3	25	7
C-1300 (Lignin)	69	260.55	179.87	50	8
LS1200 (lotus seedpod)	50.4	328.8	174.4	50	9
CL-HC (cellulose and lignin)	69	259	160.06	100	10
CPM-1100-A (peat moss)	57.5	298	157.9	50	11
CCL (corn cob lignin)	62.8	292	167	50	12
GDHC-1300 (garlic)	50.7	260	148	50	13
HHT (Lotus leaves)	66	288	126	0.2 C	14

Reference

1. C. Qiu, A. Li, D. Qiu, Y. Wu, Z. Jiang, J. Zhang, J. Xiao, R. Yuan, Z. Jiang, X. Liu, X. Chen and H. Song, *ACS Nano*, 2024, **18**, 11941-11954.
2. X. Zhang, Z. Yi, Y. Tian, L. Xie, F. Su, X. Wei, J. Chen and C.-M. Chen, *Carbon*, 2024, **226**, 119165.
3. D. Saurel, J. Segalini, M. Jauregui, A. Pendashteh, B. Daffos, P. Simon and M. Casas-Cabanas, *Energy Storage Mater.*, 2019, **21**, 162-173.
4. M. Wahid, Y. Gawli, D. Puthusseri, A. Kumar, M. V. Shelke and S. Ogale, *ACS Omega*, 2017, **2**, 3601-3609.
5. C. Nita, B. Zhang, J. Dentzer and C. Matei Ghimbeu, *J. Energy Chem.*, 2021, **58**, 207-218.
6. K. Kim, D. G. Lim, C. W. Han, S. Osswald, V. Ortalan, J. P. Youngblood and V. G. Pol, *ACS Sustainable Chem. Eng.*, 2017, **5**, 8720-8728.
7. H.-Y. Hu, Y. Xiao, W. Ling, Y.-B. Wu, P. Wang, S. J. Tan, Y. S. Xu, Y. J. Guo, W. P. Chen, R. R. Tang, X. X. Zeng, Y. X. Yin and X. W. Wu, *Energy Technol.*, 2021, **9**, 2000730.
8. S. Alvin, D. Yoon, C. Chandra, H. S. Cahyadi, J. H. Park, W. Chang, K. Y. Chung and J. Kim, *Carbon*, 2019, **145**, 67-81.
9. F. Wu, M. Zhang, Y. Bai, X. Wang, R. Dong and C. Wu, *ACS Appl. Mater. Interfaces*, 2019, **11**, 12554-12561.
10. Q. Jin, L. Tao, Y. Feng, D. Xia, G. A. Spiering, A. Hu, R. Moore, F. Lin and H. Huang, *ACS Sustainable Chem. Eng.*, 2023, **11**, 536-546.
11. J. Ding, H. Wang, Z. Li, A. Kohandehghan, K. Cui, Z. Xu, B. Zahiri, X. Tan, E. M. Lotfabad, B. C. Olsen and D. Mitlin, *ACS Nano*, 2013, **7**, 11004-11015.
12. Q. Meng, B. Chen, W. Jian, X. Zhang, S. Sun, T. Wang and W. Zhang, *J. Power Sources*, 2023, **581**, 233475.
13. H. Liu, X. Liu, H. Wang, Y. Zheng, H. Zhang, J. Shi, W. Liu, M. Huang, J. Kan, X. Zhao and D. Li, *ACS Sustainable Chem. Eng.*, 2019, **7**, 12188-12199.
14. C.-C. Wang and W. L. Su, *Surf. and Coat. Technol.*, 2021, **415**, 127125.